Magnesium-doped Biphasic Calcium Phosphate Nanoparticles with Incorporation of Silver: Synthesis, Cytotoxic and Antibacterial Properties

Ningning Yang, Peng Ding, Siyuan Wang, Shaolan Sun, Qianqian Wei, Ling Wang, Yanting Han, Okoro Oseweuba Valentine, Tianwen Wang, Guicai Li, Amin Shavandi, and Lei Nie

Abstract

The development of new calcium phosphate nanoparticles with excellent cytocompatibility and antibacterial properties is of great importance for biomedical applications. In this paper, the magnesium-doped biphasic calcium phosphate nanoparticles incorporating silver ($_{Ag}$MgB-NPs) were first synthesized by the chemical wet-precipitation method. Fourier transform infrared spectroscopy (FT-IR), X-ray diffraction (XRD), and ultraviolet-visible spectroscopy (UV-Vis) confirmed the successful synthesis of $_{Ag}$MgB-NPs. X-ray photoelectron spectroscopy (XPS) and Raman spectra indicated that Mg^{2+} was doped at the Ca^{2+} position. The good cytocompatibility of $_{Ag}$MgB-NPs was verified by cell counting kit-8 (CCK-8) analysis with culturing with human bone marrow-derived mesenchymal stem cells (hBMSCs). Additionally, the antibacterial activity of $_{Ag}$MgB-NPs was evaluated by using Gram-negative *E. coli* and Gram-positive *S. aureus*. This paper demonstrated new calcium phosphate nanoparticles for biomedical applications.

Keywords: Biomaterials; Nanoparticles; Functional; Cytocompatibility; Antibacterial Properties.

1 Introduction

Biphasic calcium phosphate (BCP) composed of hydroxyapatite (HA) and β-tricalcium phosphate (β-TCP), have been widely used for the fabrication of scaffolds in bone tissue engineering due to excellent mechanical properties, biological activity, and adjustable degradation rate [1-4]. The BCP-based scaffold with excellent antibacterial properties could be effective in preventing and treating infection

[5]. The bioactivity, biocompatibility, and antibacterial properties of BCP could be improved by incorporating ions in its chemical composition, such as manganese (Mn), selenium (Se), strontium (Sr), and so on [6-8]. Besides, the antibacterial properties of metal-doped BCP could be further increased via the deposition of silver (Ag) nanoparticles [9, 10]. Magnesium (Mg) is an abundant element in human hard tissue, including enamel, dentin, and bone [11, 12]. Mg-doped BCP nanoparticles could be produced using different methods, including chemical wet-precipitation, sol-gel, single diffusion gel, and solid-state reactions [12]. In this study, we first reported a fast and facile method to synthesize Mg-doped BCP nanoparticles (MgB-NPs) based on chemicals calcium chloride ($CaCl_2$), magnesium chloride hexahydrate ($MgCl_2{\cdot}6H_2O$), and ammonium dihydrogen phosphate ($(NH_4)_2HPO_4$), and then, silver was incorporated to obtain $_{Ag}$MgB-NPs (**Fig 1A**). the physicochemical properties of MgB-NPs and $_{Ag}$MgB-NPs were chrachterised. Furthermore, the cytocompatibility of the prepared nanoparticles was investigated by culturing with human bone marrow-derived mesenchymal stem cells (hBMSCs), and the antibacterial activity of $_{Ag}$MgB-NPs was evaluated by using Gram-negative *E. coli* and Gram-positive *S. aureus*.

2 Experimental

2.1 Fabrication of Magnesium-doped Biphasic Calcium Phosphate Nanoparticles with Incorporation of Silver ($_{Ag}$MgB-NPs)

The $_{Ag}$MgB-NPs were synthesized according to our previous reports with modification [9]. First, magnesium-doped biphasic calcium phosphate nanoparticles (MgB-NPs) was prepared. Briefly, a 50 mL mixed solution of $CaCl_2$ and $MgCl_2{\cdot}6H_2O$ was added in a three-neck flask, and a 50 mL solution of $(NH_4)_2HPO_4$ was added, the pH of the mixed solution was adjusted to 11 via adding ammonium solution. The mixed solution was stirred for 16 h, and the precipitates were collected and washed using

Millipore water. Finally, the precipitates were dried at 60 °C for 12 h to obtain MgB-NPs powder. Next, 100 mg of MgB-NPs powder was dispersed in 50 mL Millipore water in a three-neck flask, and the $AgNO_3$ was added slowly. The mixed solution was stirred for 4 h at room temperature; then the precipitates were collected and dried at 60 °C for 4 h using a vacuum drying oven to obtain $_{Ag}$MgB-NPs powder (**Fig. 1A**). Different MgB-NPs was synthesized by regulating mole ratios of Ca/Mg, and (Ca + Mg)/P (**Table. S1**), and different $_{Ag}$MgB-NPs was obtained by adjusting the mass ratio of MgB-NPs and $AgNO_3$ (**Table. S2**).

2.2 Characterizations

Dynamic light scattering (DLS, Malvern Zetasizer 3000E), cold field emission scanning electron microscope (SEM, Hitachi, S-4800), Fourier-transform infrared spectroscopy (FT-IR, PerkinElmer Spectrum 2), X-ray photoelectron spectrometer (XPS, K-Alpha 0.05 eV, Thermo Scientific), Raman spectroscopy (LabRAM HR), X-ray diffraction (XRD, Rigaku Smartlab 9 kW), and Ultraviolet-visible spectroscopy (UV-Vis) were used to evaluate the characteristics of MgB-NPs and $_{Ag}$MgB-NPs nanoparticles. In addition, Cell Counting Kit-8 (CCK-8) assay was quantitatively evaluated the cytotoxicity of MgB-NPs and $_{Ag}$MgB-NPs nanoparticles after culturing with the human bone marrow-derived mesenchymal stem cells (hBMSCs, ATCC$^{@}$PCS-500-012^{TM}). Finally, the antibacterial activity of MgB-NPs and $_{Ag}$MgB-NPs nanoparticles was evaluated by using Gram-negative *E. coli* (ATCC 25922) and Gram-positive *S. aureus* (ATCC 6538). For more details about chemicals, nanoparticles preparation and characterization, please see the Supporting Information (SI). All of the data were reported as mean ± SD (n = 5).

3 Results and discussion

Here, a facile wet coprecipitation method was used to fabricate MgB-NPs and $_{Ag}$MgB-NPs. The DLS

analysis confirmed that both MgB-NPs and $_{Ag}$MgB-NPs displayed good colloidal stability in water, and the mean diameter of each sample varied (**Fig. 1B**). SEM images confirmed that MgB-NPs and $_{Ag}$MgB-NPs displayed irregular morphology, the rodlike nanoparticles were observed, and Ag nanoparticles were clearly viewed on the surface of MgB-NPs (**Fig. 1C**). A similar morphology of MgB-NPs and $_{Ag}$MgB-NPs could be observed using TEM images (**Fig. 1S**). Next, the chemical groups of both nanoparticles were investigated by FT-IR (**Fig. 2A** and **2B**). For MgB-NPs, the typical peaks at 1087, 962, and 571 cm^{-1} correspond to the vibrational modes of the phosphate groups (PO_4^{3-}), and the broad peak centred at 3440 cm^{-1} attributed to the stretching vibration of hydrogen bond (O-H). For $_{Ag}$MgB-NPs, the absorption peak at 1455 cm^{-1} corresponded to the stretching vibration of C-O-C was observed, and it was noted that the peak at 1047 cm^{-1} disappeared compared with the spectra of MgB-NPs, which was mainly due to deposition of Ag nanoparticles on MgB-NPs. Within the combination of Raman spectra analysis (**Fig. 2S**), the Mg dopant entered the lattice of BCP, and the chemical interaction between Ag and MgB-NPs merely happened. From XPS results, the C1s, O1s, P2p, Ca2p, and Mg1s peaks were observed for MgB-NPs-1, and the additional Ag3d peak was displayed on the spectrum of $_{Ag}$MgB-NPs-1 (**Fig. 2C** and **2D**). In addition, the crystalline phases of MgB-NPs and $_{Ag}$MgB-NPs were identified using XRD (**Fig. 2E** and **2F**), two phases of HA (JCPDS No. 9-0432) and β-TCP (JCPDS, No. 9-0169) were found in all samples. Significantly, the face-centred cubic crystal structure of silver matched the peaks at (1 1 1), (2 0 0), and (2 2 0) was revealed for all $_{Ag}$MgB-NPs samples [13]. The observed broad shoulder peak with a maximum at 460 nm from UV-Vis absorption, owing to the surface plasmon resonance band (PRB) of the spherical Ag nanoparticles, confirmed the deposition of Ag nanoparticles on $_{Ag}$MgB-NPs (**Fig. 2G**).

Next, the cytotoxicity of MgB-NPs and $_{Ag}$MgB-NPs were investigated by CCK-8 assay via culturing

with hBMSCs (**Fig. 3A**, **3B**, and **3S**). The optical density (OD) values at 450 nm could quantitively evaluate the growth of hBMSCs with nanoparticles. For all samples, the OD values increased with the culturing days, indicating that hBMSCs could proliferate with nanoparticles of MgB-NPs or $_{Ag}$MgB-NPs. In addition, a similar result was obtained while using nanoparticles culturing with osteoblasts (**Fig. 4S**). Finally, the antibacterial activity of the prepared nanoparticles against *E. coli* (Gram-negative) and *S. aureus* (Gram-positive) was investigated using the Agar-well diffusion method. The antibacterial effect could be apparently observed by the presence of nanoparticles in bacterial suspension after a growth of 12 h. It was observed that the tube with the addition of sample $_{Ag}$MgB-NPs-1 displayed a transparent liquid in comparison with MgB-NPs-1 added tube, indicating $_{Ag}$MgB-NPs-1 had better antibacterial activity than MgB-NPs-1 (**Fig. 3C**). The OD at 600 nm of both bacterial suspension culturing with all samples for 12 h also confirmed the $_{Ag}$MgB-NPs could efficiently inhibit the proliferation of both bacteria than MgB-NPs (**Fig. 5S**). Based on the bacteriostatic circles' investigation (**Fig. 3D** and **6S**), $_{Ag}$MgB-NPs had significant inhibition circles against *E. coli* and *S. aureus*. The physicochemical properties, cytocompatibility, and antibacterial activity of obtained MgB-NPs and $_{Ag}$MgB-NPs were not greatly influenced by feeding mole ratios of Ca/Mg and (Ca + Mg)/P during the synthesis. The release of Ag nanoparticles from $_{Ag}$MgB-NPs is usually regulated by pH, ions concentration in the surrounding medium, such as oral, bone cavity, and so on [14]. Thus, the obtained $_{Ag}$MgB-NPs displayed potential advantages in the fabrication of scaffolds for biomedical applications, including dental application, bone regeneration, etc.

Conclusion

In summary, the nanoparticle, $_{Ag}$MgB-NPs, with excellent cytocompatibility and antibacterial

properties, were successfully synthesized using a fast and facile wet-precipitation method. The physicochemical characteristics were investigated by DLS, SEM, FT-IR, XPS, XRD, and UV-Vis. CCK-8 confirmed the excellent cytocompatibility of AgMgB-NPs after culturing with hBMSCs. Next, *E. coli* and *S. aureus* were used to validate the antibacterial activity of $_{Ag}$MgB-NPs.

Declaration of Competing Interest

The authors declare no conflict of interest.

Acknowledgements

We appreciate the assistance of Zongwen Zhang, technician of the Analysis & Testing Center of XYNU.

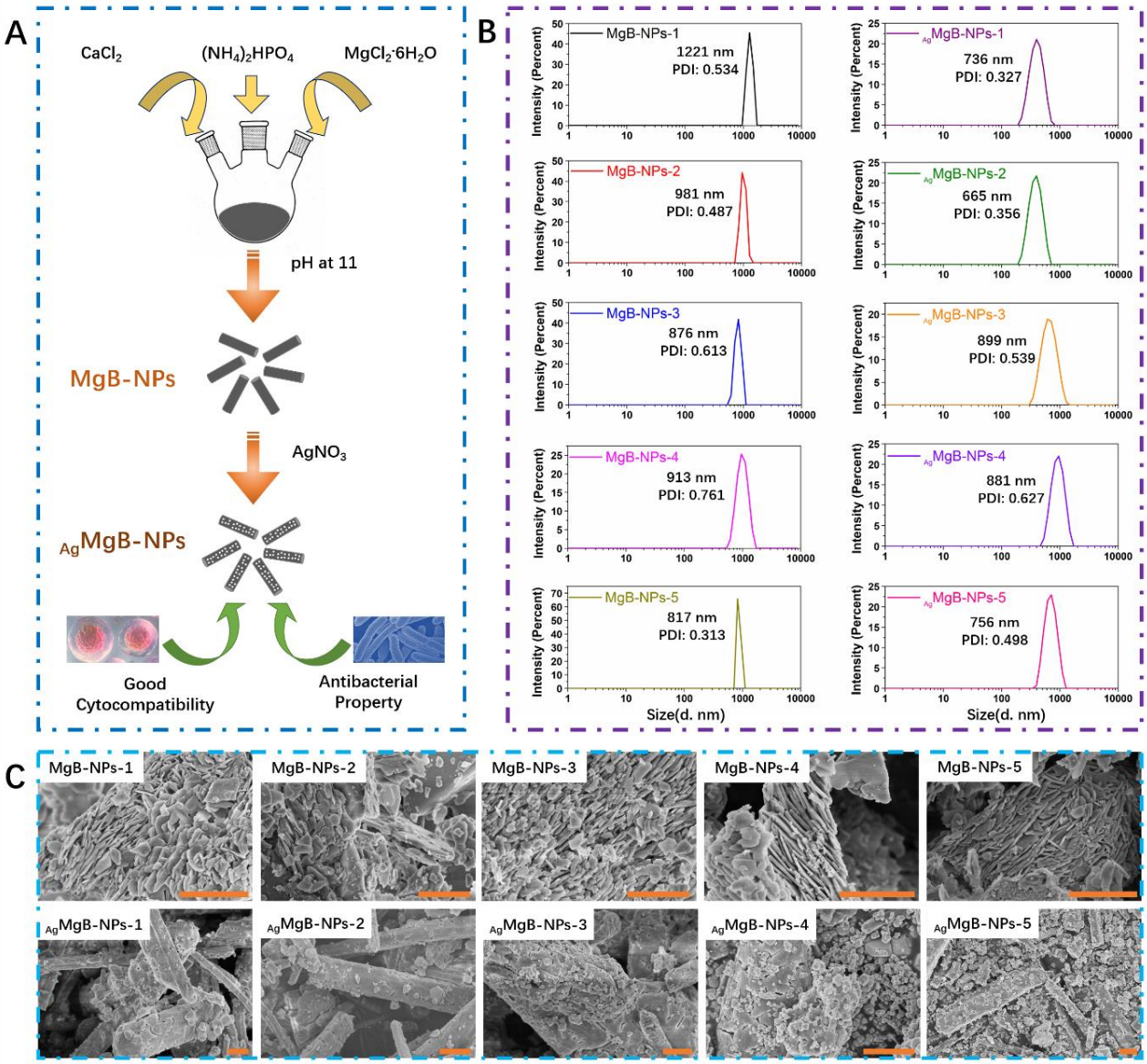

Fig. 1 (A) Schematic illustration of $_{Ag}$MgB-NPs preparation; (B) DLS analysis of prepared MgB-NPs and $_{Ag}$MgB-NPs; (C) SEM images of prepared MgB-NPs and $_{Ag}$MgB-NPs, scale bar is 2 μm.

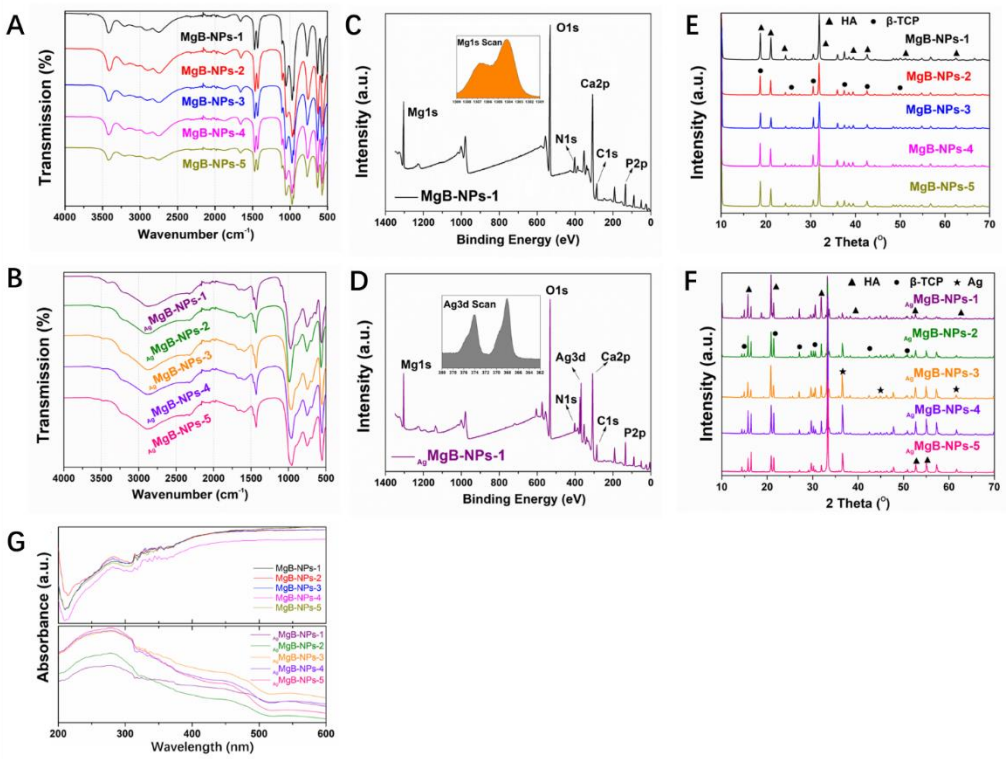

Fig. 2 FT-IR spectra of (A) MgB-NPs and (B) $_{Ag}$MgB-NPs; XPS spectra of (C) MgB-NPs-1 and (D) $_{Ag}$MgB-NPs-1; XRD spectra of (E) MgB-NPs and (F) $_{Ag}$MgB-NPs; (G) UV-Vis DRS spectra of MgB-NPs and $_{Ag}$MgB-NPs.

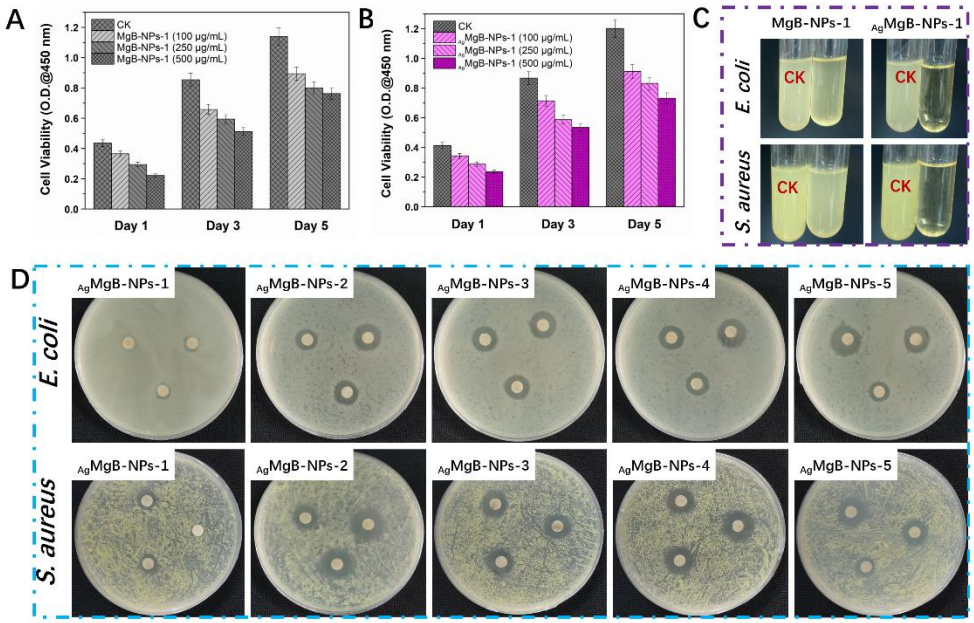

Fig. 3 (A) The cytocompatibility of (A) MgB-NPs and (B) $_{Ag}$MgB-NPs (all concentrations at 100 μg/mL) were analyzed via CCK-8 after, the absorbance at 450 nm was recorded after culturing with hBMSCs for different days, without adding nanoparticles as a control group (CK); (C) the antibacterial activity of MgB-NPs-1 and $_{Ag}$MgB-NPs-1 in cultured *E. coli* and *S. aureus* tubes (left: CK, without nanoparticles; right: supplemented with nanoparticles); (D) photos of *E. coli* and *S. aureus* grew on nutrient agar LB plates after addition of $_{Ag}$MgB-NPs (all concentrations at 500 μg/mL) for 12h.

References

[1] N. Lei, L. Xingchen, W. Zheng, H. Kehui, C. Ruihua, L. Pei, H. Yanting, S. Meng, Y. Hongyu, S. Jinping, Y. Shoufeng, In vitro biomineralization on poly(vinyl alcohol)/biphasic calcium phosphate hydrogels, Bioinspired, Biomimetic and Nanobiomaterials 9(2) (2020) 122-128.

[2] L. Nie, D. Chen, Q. Yang, P. Zou, S. Feng, H. Hu, J. Suo, Hydroxyapatite/poly-l-lactide nanocomposites coating improves the adherence and proliferation of human bone mesenchymal stem cells on porous biphasic calcium phosphate scaffolds, Materials Letters 92 (2013) 25-28.

[3] L. Nie, Y. Deng, P. Li, R. Hou, A. Shavandi, S. Yang, Hydroxyethyl Chitosan-Reinforced Polyvinyl Alcohol/Biphasic Calcium Phosphate Hydrogels for Bone Regeneration, ACS Omega 5(19) (2020) 10948-10957.

[4] L. Nie, Q. Wu, H. Long, K. Hu, P. Li, C. Wang, M. Sun, J. Dong, X. Wei, J. Suo, D. Hua, S. Liu, H. Yuan, S. Yang, Development of chitosan/gelatin hydrogels incorporation of biphasic calcium phosphate nanoparticles for bone tissue engineering, J Biomater Sci Polym Ed 30(17) (2019) 1636-1657.

[5] G.J. ter Boo, D.W. Grijpma, T.F. Moriarty, R.G. Richards, D. Eglin, Antimicrobial delivery systems for local infection prophylaxis in orthopedic- and trauma surgery, Biomaterials 52 (2015) 113-25.

[6] G.D. Webler, A.C.C. Correia, E. Barreto, E.J.S. Fonseca, Mg-doped biphasic calcium phosphate by a solid state reaction route: Characterization and evaluation of cytotoxicity, Materials Chemistry and Physics 162 (2015) 177-181.

[7] I. Sopyan, S. Ramesh, N.A. Nawawi, A. Tampieri, S. Sprio, Effects of manganese doping on properties of sol–gel derived biphasic calcium phosphate ceramics, Ceramics International 37(8) (2011) 3703-3715.

[8] S. Basu, B. Basu, Unravelling Doped Biphasic Calcium Phosphate: Synthesis to Application, ACS Applied Bio Materials 2(12) (2019) 5263-5297.

[9] L. Nie, M. Hou, T. Wang, M. Sun, R. Hou, Nanostructured selenium-doped biphasic calcium phosphate with in situ incorporation of silver for antibacterial applications, Sci Rep 10(1) (2020) 13738.

[10] L. Nie, Y. Deng, Y. Zhang, Q. Zhou, Q. Shi, S. Zhong, Y. Sun, Z. Yang, M. Sun, C. Politis, A. Shavandi, Silver-doped biphasic calcium phosphate/alginate microclusters with antibacterial property and controlled doxorubicin delivery, Journal of Applied Polymer Science 138(19) (2021) 50433.

[11] I. Cacciotti, A. Bianco, M. Lombardi, L. Montanaro, Mg-substituted hydroxyapatite nanopowders: Synthesis, thermal stability and sintering behaviour, Journal of the European Ceramic Society 29(14) (2009) 2969-2978.

[12] R. Ballouze, M.H. Marahat, S. Mohamad, N.A. Saidin, S.R. Kasim, J.P. Ooi, Biocompatible magnesium-doped biphasic calcium phosphate for bone regeneration, J Biomed Mater Res B Appl Biomater 109(10) (2021) 1426-1435.

[13] P. Bazant, I. Kuritka, L. Munster, L. Kalina, Microwave solvothermal decoration of the cellulose surface by nanostructured hybrid Ag/ZnO particles: a joint XPS, XRD and SEM study, Cellulose 22(2) (2015) 1275-1293.

[14] M. Nakamura, A. Oyane, Y. Shimizu, S. Miyata, A. Saeki, H. Miyaji, Physicochemical fabrication of antibacterial calcium phosphate submicrospheres with dispersed silver nanoparticles via coprecipitation and photoreduction under laser irradiation, Acta Biomaterialia 46 (2016) 299-307.